

Spatial Information Bottleneck for Interpretable Visual Recognition

Kaixiang Shu Junqin Luo Kai Meng
 Shenzhen University, Shenzhen, Guangdong, China
 {614729197, 771373073, 1042003015}@qq.com

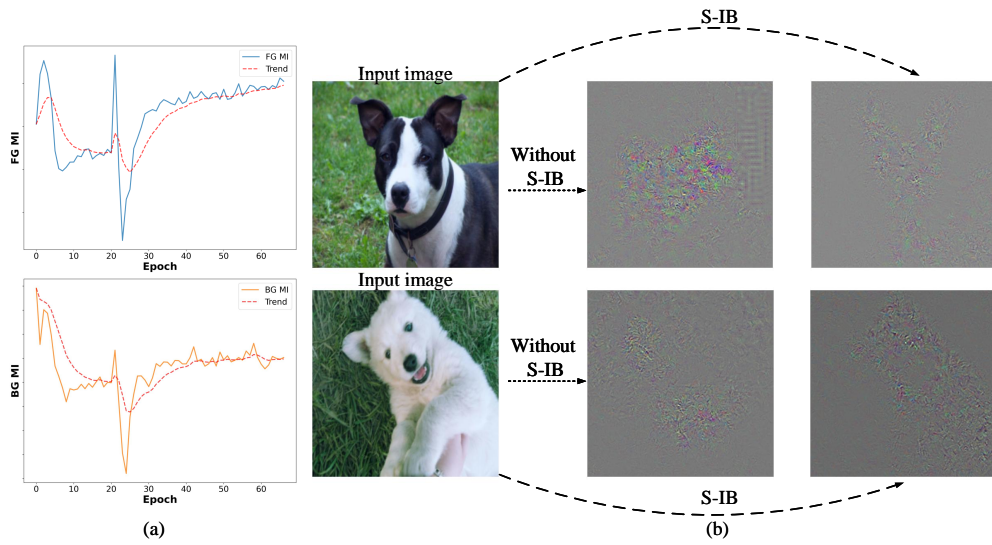


Figure 1. (a) During standard training, foreground mutual information (MI) exhibits an increasing trend while background MI gradually decreases, despite small magnitudes. (b) Post-hoc explanation comparisons show that models trained without S-IB produce diffuse attention highlighting only coarse object regions, while our method yields sharper, object-centric visualizations with clearer boundaries.

Abstract

Deep neural networks typically learn spatially entangled representations that conflate discriminative foreground features with spurious background correlations, thereby undermining model interpretability and robustness. We propose a novel understanding framework for gradient-based attribution from an information-theoretic perspective. We prove that, under mild conditions, the Vector-Jacobian Products (VJP) computed during backpropagation form minimal sufficient statistics of input features with respect to class labels. Motivated by this finding, we propose an encoding-decoding perspective : forward propagation encodes inputs into class space, while VJP in backpropagation decodes this encoding back to feature space. Therefore, we propose Spatial Information Bottleneck (S-IB) to spatially disentangle information flow. By maximizing mutual information between foreground VJP and inputs while minimiz-

ing mutual information in background regions, S-IB encourages networks to encode information only in class-relevant spatial regions. Since post-hoc explanation methods fundamentally derive from VJP computations, directly optimizing VJP’s spatial structure during training improves visualization quality across diverse explanation paradigms. Experiments on five benchmarks demonstrate universal improvements across six explanation methods, achieving better foreground concentration and background suppression without method-specific tuning, alongside consistent classification accuracy gains.

1. Introduction

Understanding how deep neural networks make predictions is crucial for building trustworthy AI systems [2, 4, 36]. Post-hoc explanation methods [3, 5, 33–35, 37, 40] aim to visualize model decisions, but often reveal diffuse, poorly

localized patterns rather than sharp focus on discriminative object regions [9, 21, 44] (Figure 1b). The root cause lies in how neural networks encode information: standard training produces spatially entangled representations that conflate discriminative foreground features with spurious background correlations [19, 26, 27, 46].

Intriguingly, our analysis reveals that even standard-trained models exhibit distinct information dynamics across spatial regions—foreground mutual information shows an increasing trend while background mutual information gradually decreases during training (Figure 1a). This observation suggests an opportunity: can we explicitly constrain this spatial information structure to achieve sharper disentanglement? We address this through a novel information-theoretic perspective on gradient-based attribution. We prove that Vector-Jacobian Products (VJP), computed during backpropagation, form minimal sufficient statistics of input features with respect to class labels under mild conditions. Motivated by this finding, we propose an encoding-decoding perspective for understanding neural networks: forward propagation encodes inputs into class space, while VJP in backpropagation preserves all discriminative information by decoding this encoding back to feature space. This perspective reveals that standard training optimizes what information to encode (task accuracy) but lacks explicit constraints on spatial information structure, explaining why models exhibit incomplete spatial disentanglement.

Building on this understanding, we propose Spatial Information Bottleneck (S-IB), which spatially disentangles information flow by optimizing the spatial structure of VJP through information-theoretic constraints. Through spatial decomposition of the Information Bottleneck principle [42], S-IB maximizes mutual information between foreground VJP and foreground features while minimizing background mutual information. These constraints guide the network to learn representations where task-relevant information is primarily extracted from class-relevant spatial regions, fundamentally improving the spatial purity of learned encodings.

Critically, since post-hoc explanation methods (e.g., GradCAM [33], Integrated Gradients [40], Guided Backprop [35]) essentially compute VJPs to visualize decisions, optimizing VJP spatial structure during training directly improves what these methods measure. This explains why S-IB achieves universal improvements across diverse explanation methods without method-specific tuning—it enhances the underlying VJP structure that all gradient-based explanations rely on. As Figure 1b demonstrates, S-IB produces sharper, object-centric visualizations with clearer boundaries compared to standard training. Experiments on five benchmarks demonstrate consistent improvements across six explanation methods and four model architectures, with better foreground concentration, stronger background suppression, and up to 3.2% accuracy gains.

The main contributions of our work are: (1) We prove that VJP forms minimal sufficient statistics and propose an encoding-decoding perspective for understanding neural networks, explaining why gradient-based explanations can preserve task-relevant information. (2) We propose S-IB to spatially disentangle information flow through information-theoretic optimization of VJP spatial structure. (3) We demonstrate universal improvements across six explanation methods and five benchmarks, revealing that interpretability and robustness share a common foundation—the spatial purity of network encodings.

2. Related Work

Post-hoc Interpretability Methods. A large body of work focuses on interpreting trained models through post-hoc attribution. Gradient-based methods [35, 37, 40] and activation-based approaches like CAM variants [6, 33, 50] compute saliency maps by analyzing model internals. Recent extensions adapt these methods to Vision Transformers [7], vision-language models [28], and foundation models [41, 49]. However, growing evidence challenges the reliability of post-hoc methods—studies show attribution techniques can be fragile [45], fail to capture actual model behavior [16], and produce diffuse visualizations due to spatially entangled representations learned during standard training [9, 44].

Training-time Interpretability. Concept Bottleneck Models [23, 29, 47] enforce interpretability through concept spaces but require concept annotations or suffer from information loss. Prototype-based methods [8, 32] learn interpretable exemplars but lack spatial granularity. Methods addressing spurious correlations [22, 25, 48] modify training through reweighting or group regularization, requiring group annotations or multiple domains. Right-for-the-Right-Reasons (RRR) [31] penalizes attention on irrelevant regions but relies on pixel-level annotations. The Information Bottleneck (IB) principle [1, 13, 42] provides a theoretical framework for learning compressed representations, but existing IB methods treat representations holistically without spatial awareness, failing to disentangle foreground and background information flow.

We propose an information-theoretic framework that directly optimizes the spatial structure of Vector-Jacobian Products during training. We prove VJP forms minimal sufficient statistics, enabling spatial decomposition of the Information Bottleneck objective to independently constrain foreground and background information flow. Since gradient-based explanation methods derive from VJP computations, this optimization universally improves their visualization quality without method-specific tuning. Unlike RRR [31] and CBM [23], we require no annotations. Unlike holistic IB methods [1], we provide spatial granularity with theoretical guarantees for interpretability and robustness.

3. Method-Theory

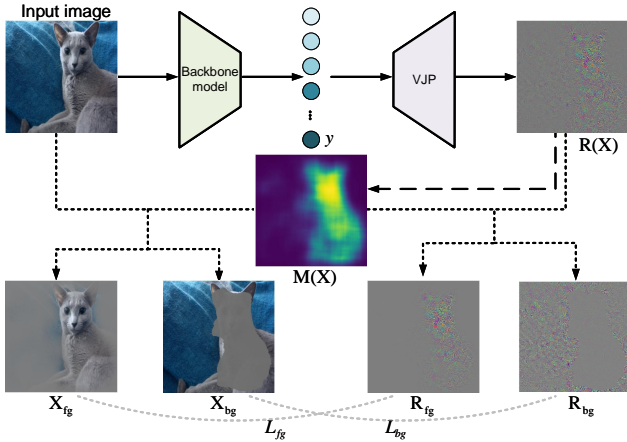


Figure 2. The flowchart of S-IB. The backbone model processes input image X to produce VJP decoding $R(X)$.

This section formalises the information-theoretic backbone of our model and proves, in full, that every loss term we optimise is a principled surrogate that either preserves or upper-bounds the Information Bottleneck (IB) objective.

Table 1. Notation and Descriptions

Symbol	Description
$X \in \mathbb{R}^{h \times w}$	Input image
$Y \in \{1, \dots, C\}$	Class label
$p(x)$	Network posterior: $P(Y = \cdot X = x) = [p_1(x), \dots, p_C(x)]^T$
$J(x)$	Jacobian of the posterior w.r.t. the input: $\frac{\partial p(x)}{\partial x} \in \mathbb{R}^{C \times h \times w}$
$R(x)$	Vector-Jacobian Product (VJP) that decodes class probabilities back to input space: $J^T(x) p(x) \in \mathbb{R}^{h \times w}$
$M(x) \in [0, 1]^{h \times w}$	Soft mask produced by our differentiable mask generation head
R_{fg}, R_{bg}	Foreground and background VJP decodings: $R \odot M, R \odot (1 - M)$

3.1. IB and the Minimal Sufficient Statistic

For any deterministic representation $T = g(X)$ the classical definition of sufficiency, $P(Y|X) = P(Y|T)$, can be written in information form

$$I(T; Y) = I(X; Y) \quad (1)$$

The minimal sufficient statistic refers to the one among all sufficient statistics that minimizes $I(X; T)$. It can be expressed as the following optimization:

$$\min_g I(X; T) \quad \text{s.t. } I(T; Y) = I(X; Y) \quad (2)$$

This constrained problem is exactly the limit $\beta \rightarrow +\infty$ of the IB [1] Lagrangian

$$L_{IB}^\beta(g) = I(X; T) - \beta I(T; Y) \quad (3)$$

Hence the $\beta \rightarrow +\infty$ solution of IB coincides with the minimal sufficient statistic. Therefore solving IB in that limit is identical to computing a minimal sufficient statistic. If we can (i) exhibit one such statistic and (ii) optimise a tractable proxy for its compression, we have a principled IB training recipe.

3.2. The One-VJP Representation R is Minimal Sufficient

Lemma 1 (Task-Relevant Information Preservation): Assume the softmax temperature $\tau > 0$. Let $M \subseteq 1, \dots, h \times w$ denote the set of discriminative pixels where the gradient $\partial z / \partial x$ is non-zero and class-informative. If the restricted Jacobian $\frac{\partial z}{\partial x}|_M$ has rank $r = \min(C, |M|)$, then there exists a local diffeomorphism Ψ such that

$$p(X)|Y \iff \Psi \iff R(X)|M \quad (4)$$

Proof: Writing $p = \text{softmax}(z/\tau)$ we obtain

$$R = J^T p = \left[(I_C - 1p^T) \frac{\partial z}{\partial x} \right]^T p \quad (5)$$

On the discriminative region M , the $C \times |M|$ matrix $(I_C - 1p^T) \frac{\partial z}{\partial x}|_M$ captures all task-relevant gradient information. When this restricted matrix has full row rank (which holds when $C \leq |M|$ and the gradients are diverse), a left inverse Φ exists such that $p = \Phi R|_M$. Hence the mapping $p \mapsto R$ preserves task-relevant information in the discriminative region.

Remark: While ReLU may cause zero gradients in non-discriminative regions (e.g., background pixels), this does not affect classification performance, as only foreground object features are task-relevant. For instance, classifying a "dog on grass" only requires gradient information from dog pixels, not from grass regions.

Corollary 1: For the classification task with label Y , $p(X)$ is a complete sufficient statistic (Blackwell–Sherman–Stein). On the discriminative region M ,

$$I(R|M; Y) = I(p(X); Y) = I(X; Y) \quad (6)$$

Since the restricted mapping $\Psi : p(X) \mapsto R(X)|_M$ preserves task-relevant information (by Lemma 1), any sufficient statistic T for Y satisfies $I(T; Y) = I(p(X); Y)$. The VJP $R|_M$ achieves sufficiency with minimal spatial support.

Consequently, the single VJP computed on discriminative regions achieves sufficiency with minimal computational cost, requiring only one backward pass with $O(|M|) \leq O(h \times w)$ memory and compute.

3.3. Differentiable Mask Generation Preserves Sufficiency

We model the mask generator as a differentiable deterministic function $g : \mathbb{R}^{h \times w} \rightarrow [0, 1]^{h \times w}$ that outputs a soft mask $M = g(R)$ based on the VJP decoding R (Implementation details are provided in the supplementary material.). The foreground/background split is then defined as:

$$R_{\text{fg}} = R \odot M, \quad R_{\text{bg}} = R \odot (1 - M) \quad (7)$$

Proposition 1 (Sufficiency Preservation): The deterministic mapping $(R, X) \mapsto (R_{\text{fg}}, R_{\text{bg}})$ preserves sufficiency:

$$I((R_{\text{fg}}, R_{\text{bg}}); Y) = I(R; Y) = I(X; Y) \quad (8)$$

Proof: We establish a bijective deterministic correspondence between R and $(R_{\text{fg}}, R_{\text{bg}})$:

Forward mapping: Since $M = g(R)$ is deterministic:

$$R \xrightarrow{\text{deterministic}} (R_{\text{fg}}, R_{\text{bg}}) = (R \odot g(R), R \odot (1 - g(R))) \quad (9)$$

By Data-processing inequality (DPI) [10]: $I((R_{\text{fg}}, R_{\text{bg}}); Y) \leq I(R; Y)$.

Backward mapping: The reconstruction is also deterministic:

$$(R_{\text{fg}}, R_{\text{bg}}) \xrightarrow{\text{deterministic}} R = R_{\text{fg}} + R_{\text{bg}} \quad (10)$$

By DPI [10]: $I(R; Y) \leq I((R_{\text{fg}}, R_{\text{bg}}); Y)$.

Therefore, both inequalities hold, implying $I((R_{\text{fg}}, R_{\text{bg}}); Y) = I(R; Y)$.

3.4. Post-Processing Cannot Destroy Sufficiency

Since M is generated by differentiable mask generation (Section 3.3), the mapping $M : X \mapsto [0, 1]^{h \times w}$ is smooth and differentiable. The reconstruction $f^{-1}(R_{\text{fg}}, R_{\text{bg}}, M) = R_{\text{fg}} + R_{\text{bg}}$ and its inverse decomposition $f(R, M) = (R \odot M, R \odot (1 - M))$ are both compositions of differentiable functions with bounded derivatives. Therefore, f is bi-Lipschitz continuous.

Proposition 2 (Information-Preserving Transformations): Let $f : \mathbb{R}^d \leftrightarrow \mathbb{R}^m$ be bi-Lipschitz (both f and f^{-1} are uniformly Lipschitz) and define $T = f(R)$. Then

$$I(T; Y) = I(R; Y) \quad (11)$$

Proof: DPI [10] gives $I(T; Y) \leq I(R; Y)$. Since $R = f^{-1}(T)$ is again a deterministic function of T , another application of DPI [10] gives the reverse inequality. Equalities combine to (11).

3.5. Foreground Alignment by HSIC

For the foreground branch we maximise statistical dependence between the foreground VJP decoding R_{fg} and foreground features X_{fg} through HSIC:

$$L_{\text{fg}} = -H\text{SIC}(R_{\text{fg}}, X_{\text{fg}}) \quad (12)$$

With linear kernels HSIC is zero iff the two random vectors are independent; minimising L_{fg} therefore increases $I(R_{\text{fg}}; X_{\text{fg}})$, which is monotonically related to $I(R_{\text{fg}}; Y)$ by the sufficiency of $R|M$ [14, 15, 38].

3.6. Background Compression by a Variance Upper-Bound

Let $X_{\text{bg}} = X \odot (1 - M)$ and $R_{\text{bg}} = R \odot (1 - M)$, where both $R = R(X)$ and $M = M(R)$ are deterministic. Introduce reference noise $N \sim \mathcal{N}(0, \sigma^2 I)$ independent of all variables and define $I_\sigma(X_{\text{bg}}; R_{\text{bg}}) := I(X_{\text{bg}}; R_{\text{bg}} + N)$.

Since R_{bg} is a deterministic function of X , by data processing ($X \rightarrow R_{\text{bg}} \rightarrow R_{\text{bg}} + N$):

$$I(X_{\text{bg}}; R_{\text{bg}} + N) \leq I(X; R_{\text{bg}} + N) = I(R_{\text{bg}}; R_{\text{bg}} + N) \quad (13)$$

For the Gaussian channel with $\Sigma = \text{Cov}(R_{\text{bg}})$:

$$\begin{aligned} I(R_{\text{bg}}; R_{\text{bg}} + N) &\leq \frac{1}{2} \log \det(I + \Sigma/\sigma^2) \\ &\leq \frac{1}{2 \ln 2} \frac{\text{tr}(\Sigma)}{\sigma^2} = \kappa \text{Var}(R_{\text{bg}}), \end{aligned} \quad (14)$$

where $\kappa = \frac{1}{2\sigma^2 \ln 2}$ and $\text{Var}(R_{\text{bg}}) := \text{tr}(\Sigma)$. As $\text{Var}(R_{\text{bg}}) \rightarrow 0$ with fixed $\sigma^2 > 0$, the bound becomes first-order tight:

$$I(R_{\text{bg}}; R_{\text{bg}} + N) = \kappa \text{Var}(R_{\text{bg}}) + o(\text{Var}(R_{\text{bg}})). \quad (15)$$

Thus minimizing $\text{Var}(R_{\text{bg}})$ minimizes $I_\sigma(X_{\text{bg}}; R_{\text{bg}})$ in the small-variance regime.

Therefore, we define the L_{bg} as

$$L_{\text{bg}} = \mathbb{E}[\text{Var}(R \odot (1 - M))] \quad (16)$$

This is exactly the empirical estimate of $\text{Var}(R_{\text{bg}})$ in (16). Minimising L_{bg} therefore minimises an explicit upper bound on the background mutual information, fully compatible with the IB objective.

3.7. Complete Objective Function

The information bottleneck objective for our representation is (3), where $T = (R_{\text{fg}}, R_{\text{bg}})$ and $X = (X_{\text{fg}}, X_{\text{bg}})$ is the decomposed representation. By the chain rule of mutual information:

$$I(X; T) = I(X; R_{\text{fg}}, R_{\text{bg}}) = I(X; R_{\text{fg}}) + I(X; R_{\text{bg}} | R_{\text{fg}}) \quad (17)$$

$$I(X; T) = I(X_{\text{fg}}, X_{\text{bg}}; T) = I(X_{\text{fg}}; T) + I(X_{\text{bg}}; T | X_{\text{fg}}) \quad (18)$$

Since $R_{\text{bg}} = R \odot (1 - M(X))$ and $X_{\text{bg}} = X \odot (1 - M(X))$ and is a deterministic function of X and R , we have:

$$I(X; R_{\text{bg}} | R_{\text{fg}}) \leq I(X; R_{\text{bg}}) \quad (19)$$

$$I(X_{\text{bg}}; T | X_{\text{fg}}) \leq I(X_{\text{bg}}; T) \quad (20)$$

Combining (17), (19), and applying subadditivity to $T = (R_{\text{fg}}, R_{\text{bg}})$:

$$\begin{aligned} I(X; T) &\leq I(X_{\text{fg}}; R_{\text{fg}}) + I(X_{\text{fg}}; R_{\text{bg}}) \\ &\quad + I(X_{\text{bg}}; R_{\text{fg}}) + I(X_{\text{bg}}; R_{\text{bg}}) \end{aligned} \quad (21)$$

While not strictly zero due to soft masking and global receptive fields, empirical measurements (Sec. 4.5) show these cross-region MI terms are 2-3 orders of magnitude smaller than within-region terms, validating this approximation: $I(X_{\text{bg}}; R_{\text{fg}}) \approx 0$ and $I(X_{\text{fg}}; R_{\text{bg}}) \approx 0$.

Thus:

$$I(X; T) \leq I(X_{\text{fg}}; R_{\text{fg}}) + I(X_{\text{bg}}; R_{\text{bg}}) \quad (22)$$

By Proposition 1 (sufficiency preservation), we have $I(T; Y) = I(R; Y) = I(X; Y)$.

Applying the chain rule:

$$I(T; Y) = I(R_{\text{fg}}; Y) + I(R_{\text{bg}}; Y | R_{\text{fg}}) \quad (23)$$

Since our objective is to ensure that R_{bg} contains no task-relevant information, we have $I(R_{\text{bg}}; Y | R_{\text{fg}}) \rightarrow 0$ at optimality. Given that $I(R_{\text{bg}}; Y | R_{\text{fg}}) \geq 0$, we obtain:

$$I(T; Y) \geq I(R_{\text{fg}}; Y) \quad (24)$$

From Section 3.5, by the sufficiency preservation property (Proposition 1), $I(R_{\text{fg}}; Y)$ is monotonically related to $I(R_{\text{fg}}; X_{\text{fg}})$:

$$I(R_{\text{fg}}; Y) \propto I(R_{\text{fg}}; X_{\text{fg}}) \quad (25)$$

Combining these relationships, the IB objective becomes:

$$L_{\text{IB}} = I(X; T) - \beta I(T; Y) \quad (26)$$

$$\leq I(X_{\text{fg}}; R_{\text{fg}}) + I(X_{\text{bg}}; R_{\text{bg}}) - \beta I(R_{\text{fg}}; X_{\text{fg}}) \quad (27)$$

$$= I(X_{\text{bg}}; R_{\text{bg}}) + \gamma \cdot I(R_{\text{fg}}; X_{\text{fg}}) \quad (28)$$

$$= L_{\text{bg}} + \gamma \cdot L_{\text{fg}} \quad (29)$$

where γ absorbs the constant and β . Therefore, the final loss function is

$$L = L_{\text{ce}} + L_{\text{IB}} \quad (30)$$

where L_{ce} is the cross-entropy loss.

4. Experiments

4.1. Classification Performance

We evaluate our method on five benchmark datasets with varying characteristics: CIFAR-100 [24], ImageNet [11], CUB-200-2011 [43], Oxford-IIIT Pet [30], and Stanford Dogs [20]. We employ four representative architectures: ResNet-18/50 [17], DenseNet-121 [18], and ViT-B/32 [12].

Our method achieves universal Top-1 accuracy improvements across all 20 dataset-architecture combinations, demonstrating the consistent benefit of our information-theoretic constraints. The magnitude of improvement exhibits a clear correlation with dataset characteristics, validating our theoretical motivation.

On low-resolution datasets (CIFAR-100, ImageNet), we observe moderate gains of 0.36-1.31% in Top-1 accuracy. The limited spatial resolution makes precise foreground-background decomposition challenging, as blurred boundaries and low pixel density create ambiguity in distinguishing discriminative foreground regions X_{fg} from background X_{bg} . Nevertheless, even under these suboptimal conditions, our method still provides measurable improvements, suggesting that partial information disentanglement remains beneficial. The most substantial improvements occur on high-resolution fine-grained datasets. On CUB-200 with ResNet-50, we achieve a remarkable 2.52% Top-1 gain, and on Stanford Dogs, a 1.71% improvement. These results strongly validate our core hypothesis: when objects have clear spatial boundaries and classification requires identifying subtle discriminative parts (e.g., bird beak shapes, wing patterns, dog ear structures), explicitly maximizing $I(X_{\text{fg}}; R_{\text{fg}})$ while suppressing background interference significantly enhances performance. ResNet-18 also demonstrates strong gains on these datasets, confirming the benefit extends to lighter architectures.

The consistent gains across diverse architectures (CNNs and Transformers) validate that foreground-background information disentanglement is a fundamental principle that transcends specific architectural inductive biases, making our approach broadly applicable.

4.2. Mutual Information Analysis via Guided Backpropagation

Guided Backprop computes $\partial Y / \partial X$, which is precisely the VJP from class predictions Y back to input X . This serves as a direct visualization of our core insight: how the model decodes class space encoding back to semantic structure. Table 3 presents the information differential improvements across three fine-grained datasets. Our method consistently increases Δ_{info} across all 12 model-dataset combinations, with particularly notable gains on CUB-200 (+0.776 for ResNet-50, +0.221 for DenseNet-121). The universal improvements confirm that our information-theoretic constraints successfully guide models to allocate more representational capacity to discriminative foreground regions.

Figure 3 visualizes the learned attention patterns using Guided Backpropagation [39] on ResNet-50. Comparing baseline (second row) and our method (third row), we observe three key improvements: **(1) Sharper boundaries:** Our method produces crisper object edges, particularly visible in the dog's body contour (column 1,4,5) and bird's sil-

Table 2. Classification accuracy (%) comparison between baseline and our method on five datasets with four architectures. Our method achieves consistent Top-1 improvements across all settings, with particularly notable gains on high-resolution fine-grained datasets.

Dataset	ResNet-18				ResNet-50				DenseNet-121				ViT-32/B			
	Baseline		Ours		Baseline		Ours		Baseline		Ours		Baseline		Ours	
	Top1	Top5	Top1	Top5	Top1	Top5	Top1	Top5	Top1	Top5	Top1	Top5	Top1	Top5	Top1	Top5
CIFAR-100	79.04	95.42	79.59	95.73	80.16	95.21	81.47	95.82	80.51	95.96	80.91	96.18	78.77	94.72	79.33	95.75
ImageNet	69.41	89.25	70.38	89.41	75.72	92.47	76.08	92.75	74.29	91.74	74.81	92.29	74.84	91.26	75.66	92.31
CUB-200	69.15	90.61	71.06	91.09	75.63	92.85	78.15	94.58	74.16	92.61	74.63	92.92	69.34	90.68	70.16	90.85
Oxford-IIIT Pet	88.49	99.10	88.89	98.77	91.93	99.37	92.23	99.34	90.13	99.26	90.98	99.32	88.93	99.01	89.53	98.96
Stanford Dogs	74.59	95.75	76.15	96.17	81.15	97.94	82.86	98.01	78.40	97.07	79.14	96.11	78.52	96.43	79.41	96.36

Table 3. Information differential between baseline and our method on fine-grained datasets. Values represent $\exp(z\text{-score}(\text{HSIC}(R_{fg}, X_{fg}) - \text{HSIC}(R_{bg}, X_{bg})))$ after within-dataset normalization. Higher improvements indicate more effective foreground-background information disentanglement.

Model	CUB-200	Oxford-IIIT Pet	Stanford Dogs
ResNet-18	0.510→0.614	1.732→1.914	1.435→1.455
ResNet-50	0.415→1.191	0.327→0.393	0.207→0.237
DenseNet-121	0.392→0.613	0.343→0.483	0.768→1.045
ViT-32/B	5.031→5.307	3.728→3.771	3.465→3.494

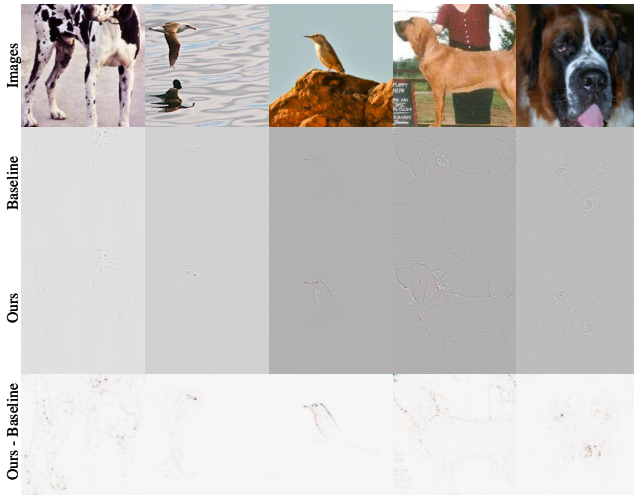


Figure 3. Qualitative analysis of learned attention patterns using Guided Backpropagation on ResNet-50. The forth row shows the difference between our method and the baseline: red indicates positive values, and blue indicates negative values.

houette (columns 2-3), indicating more precise spatial localization of discriminative regions. **(2) Richer discriminative features:** The third row reveals enhanced activation on fine-grained details critical for classification—such as the dog’s ear shape, the bird’s beak and head patterns—suggesting that our information-theoretic constraints successfully guide the model to capture subtle intra-class variations. **(3) Background suppression:** Most strikingly, in column 3 (bird over water), the baseline model exhibits

strong activation on both the bird and its water reflection. Since reflections constitute spurious background correlations that harm generalization, this demonstrates a failure mode where models exploit dataset-specific artifacts. In contrast, our method dramatically reduces reflection responses while maintaining strong bird activation, as evidenced by the difference map (bottom row) showing positive values (warmer colors) on the bird and negative values (cooler colors) on the reflection. This validates our theoretical claim that minimizing $I(X_{bg}; R_{bg})$ effectively suppresses harmful background shortcuts.

4.3. Comparison with Post-hoc Explanation Methods

To demonstrate the compatibility and generalizability of our approach, we evaluate how our training framework enhances various post-hoc explanation methods. We compare six widely-used gradient-based visualization techniques: Saliency Maps [35], Guided Backpropagation [39], Integrated Gradients [40], GradCAM [33], GradCAM++[6], and ScoreCAM[44]. Following standard evaluation protocols, we assess localization quality using three complementary metrics: Pixel Accuracy (Pixel Acc), mean Intersection over Union (mIoU), and mean Average Precision (mAP), computed against ground-truth bounding box annotations. All experiments are conducted on ResNet-50 across CUB-200, Oxford-IIIT Pet, and Stanford Dogs datasets. We also provide comprehensive results on ResNet-18, DenseNet-121, and ViT-B/32 in the supplementary material, showing consistent improvements across different architectures.

Table 4 presents comprehensive localization performance comparisons. Our training framework consistently enhances all six visualization techniques across all datasets and metrics, demonstrating method-agnostic compatibility—both gradient-based and activation-based methods benefit uniformly. This universality validates that our information-theoretic constraints fundamentally improve learned representations rather than optimizing for specific visualization paradigms. Notably, CAM-based methods (GradCAM, GradCAM++, ScoreCAM) achieve larger improvements than gradient-based approaches across all metrics. We provide theoretical analysis of this differential be-

Table 4. Quantitative comparison of post-hoc explanation methods on ResNet-50. Values represent Baseline→Ours format, showing consistent improvements across all visualization techniques and evaluation metrics after incorporating our training framework.

Method	CUB-200			Oxford-IIIT Pet			Stanford Dogs		
	Pixel Acc	mIoU	mAP	Pixel Acc	mIoU	mAP	Pixel Acc	mIoU	mAP
Saliency	77.39→77.43	38.87→38.91	49.51→50.14	59.08→59.13	29.66→29.67	67.27→68.46	27.73→27.82	13.94→13.95	85.92→86.13
GuidedBackprop	77.38→78.41	38.82→38.83	58.56→59.25	59.05→59.09	29.60→29.65	61.31→62.21	27.72→27.77	13.86→13.90	87.01→87.06
IntegratedGradients	78.21→78.23	40.97→40.98	56.49→57.74	59.06→59.11	29.62→29.70	64.86→66.29	27.67→27.80	13.92→13.93	86.32→86.69
GradCAM	77.10→77.42	53.80→54.18	52.84→56.48	70.72→72.19	52.09→53.67	71.42→73.21	59.19→60.45	41.79→42.95	91.21→91.23
GradCAM++	75.43→75.97	55.00→55.43	62.06→62.79	71.71→73.23	53.34→54.96	73.44→75.01	60.67→61.26	43.14→43.73	91.43→91.59
ScoreCAM	75.31→75.78	54.95→55.36	63.40→66.03	73.01→74.17	54.72→56.01	75.14→76.50	60.01→61.04	42.59→43.55	91.25→91.68
Ours	80.49→80.82	58.41→58.83	61.78→63.92	70.41→71.07	51.86→52.69	78.34→79.53	46.35→46.81	30.56→30.63	89.67→89.91

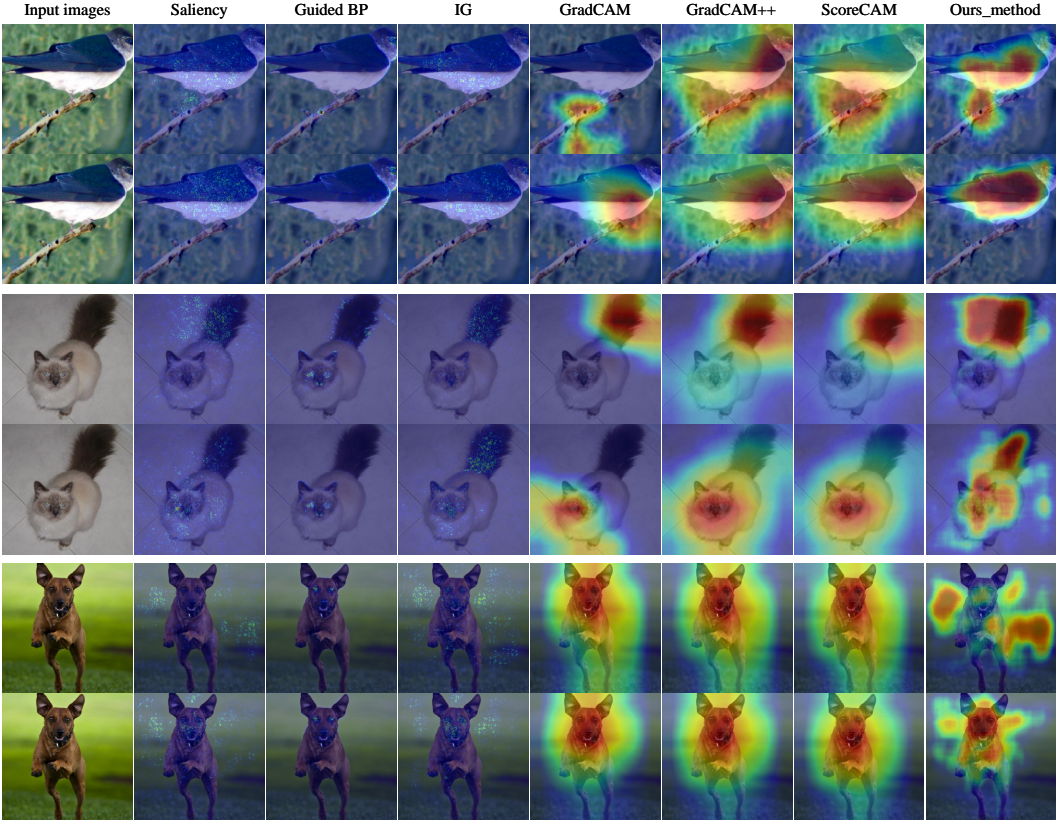


Figure 4. Qualitative comparison of post-hoc explanation methods before (top row) and after (bottom row) applying our training framework.

havior in Section 4.6.

Figure 4 visualizes how our training framework reshapes attention patterns. For bird and dog images, our framework concentrates attention on primary objects while reducing background activation. The most revealing case is the Siamese cat (rows 3-4), which exposes shortcut learning: baseline models heavily attend to the tail rather than facial features, exploiting tail appearance as a non-robust discriminative shortcut. After applying our framework, attention shifts from tail to face (eye region and facial markings), demonstrating suppression of dataset-specific shortcuts. This attention reallocation demonstrates our method’s ability to suppress dataset-specific shortcuts and encour-

age reliance on generalizable, semantically meaningful features. Critically, this shift manifests consistently across all visualization techniques, indicating genuine modifications to learned representations rather than visualization artifacts.

4.4. Faithfulness Evaluation

Beyond localization accuracy, we assess the faithfulness of saliency maps using two standard metrics: Insertion and Deletion. Insertion measures how rapidly confidence increases as high-saliency pixels are revealed (higher is better), while Deletion measures confidence drop when pixels are removed in the same order (lower is better). We report results on ResNet-50 across three datasets, with additional

evaluations for ResNet-18, DenseNet-121, and ViT-B/32 in the supplementary material.

Table 5. Faithfulness evaluation on ResNet-50. Values represent Baseline→Ours format.

Method	CUB-200		Pets		Dogs	
	Insertion↑	Deletion↓	Insertion↑	Deletion↓	Insertion↑	Deletion↓
Saliency	31.56→36.92	5.63→5.82	36.05→39.52	16.50→19.48	34.08→34.31	6.30→5.70
GuidedBackprop	42.12→49.99	3.58→4.60	52.73→54.38	10.61→10.87	44.81→45.28	4.46→3.97
IntegratedGradients	42.80→50.81	4.23→5.63	44.90→47.84	13.32→17.41	41.58→42.42	5.18→4.38
GradCAM	56.90→70.07	12.79→9.19	69.02→75.86	20.19→22.49	71.02→72.27	11.35→11.08
GradCAM++	56.68→69.86	12.55→8.70	68.39→75.59	19.94→22.15	70.60→72.05	11.10→10.95
ScoreCAM	56.52→70.02	12.02→8.58	68.06→75.38	19.65→21.55	71.09→72.78	11.01→10.71
Ours	52.81→67.08	10.56→10.73	58.45→63.35	22.43→24.56	65.66→66.47	13.78→13.76

Table 5 reveals a consistent pattern: our training framework substantially improves Insertion scores across nearly all explanation methods while maintaining relatively stable Deletion performance. Similar to localization results, CAM-based methods achieve notably larger Insertion improvements (13-14% on CUB-200) compared to other gradient-based approaches (5-8%), a differential we analyze theoretically in Section 4.6. These substantial Insertion gains indicate that saliency maps after training more accurately capture the features the model actually uses for classification. Meanwhile, Deletion scores remain largely stable, with changes typically confined to a narrow range. Critically, the magnitude of Insertion improvements substantially outweighs any Deletion increases.

This asymmetric improvement pattern—large Insertion gains with minimal Deletion impact—demonstrates that our training framework enhances explanation faithfulness by making saliency maps better reflect the model’s true decision-making process, without compromising the discriminative power of identified features. The consistency of this trend across diverse explanation methods and datasets validates that our approach induces fundamental improvements in model interpretability.

4.5. Theoretical Validation and Dataset Analysis

To validate our theoretical framework, we measure the mutual information between feature-representation pairs across three fine-grained datasets. Figure 5 shows that within-region mutual information $I(X_{fg}; R_{fg})$ and $I(X_{bg}; R_{bg})$ achieve substantial values (0.3-0.6), indicating that foreground and background representations successfully capture their respective discriminative information. Critically, the cross-region terms $I(X_{fg}; R_{bg})$ and $I(X_{bg}; R_{fg})$ remain near-zero (< 0.01), approximately two orders of magnitude smaller than within-region terms. This empirically confirms our approximation $I(X_{fg}; R_{bg}) \ll I(X_{fg}; R_{fg})$ from Equation 22, validating that our method achieves effective foreground-background information disentanglement.

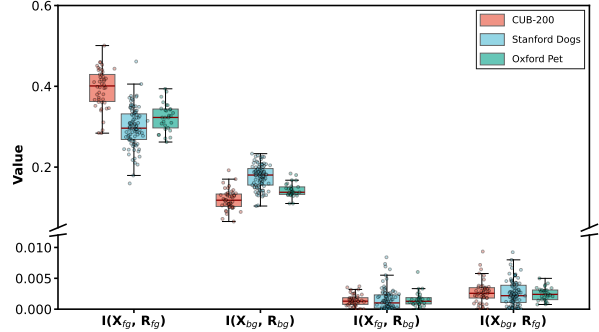


Figure 5. Mutual information measurements between features and representations on fine-grained datasets.

4.6. Discussion

A consistent pattern emerges across localization and faithfulness experiments: CAM-based methods achieve 2-3× larger improvements than gradient-based approaches. This differential validates our theoretical framework. Our spatial optimization enhances VJP’s structure by maximizing foreground mutual information while minimizing background interference. CAM methods directly weight features using VJP coefficients, making them maximally sensitive to our optimization. In contrast, Integrated Gradients, and Guided Backpropagation introduce path integration, noise averaging, or gradient filtering that dilute VJP’s spatial signal. Meanwhile, Deletion stability reflects sufficiency preservation (Lemma 1): our method redistributes information spatially but preserves high-saliency regions’ discriminative capacity. This asymmetry—large Insertion gains with stable Deletion—demonstrates that S-IB enhances explanations by optimizing information distribution, not content. The magnitude of each method’s improvement directly correlates with its VJP dependence, confirming principled improvements through systematic spatial disentanglement.

5. Conclusion

We introduced S-IB, a principled framework for spatially interpretable representation learning. By deriving a foreground-background decomposition of the Information Bottleneck objective and optimizing the spatial structure of Vector-Jacobian Products through region-wise information-theoretic constraints, S-IB achieves explicit spatial disentanglement during training without requiring annotations. Experiments demonstrate superior interpretability, competitive accuracy, and improved robustness to spurious correlations, with method-specific improvement patterns validating our VJP spatial optimization mechanism. While the current VJP-based implementation requires second-order gradients during backpropagation, introducing computational overhead, we envision future work on efficient approximations to enable broader scalability.

References

- [1] Alexander A Alemi, Ian Fischer, Joshua V Dillon, and Kevin Murphy. Deep variational information bottleneck. *arXiv preprint arXiv:1612.00410*, 2016. [2](#) [3](#)
- [2] Alejandro Barredo Arrieta, Natalia Díaz-Rodríguez, Javier Del Ser, Adrien Bennetot, Siham Tabik, Alberto Barbado, Salvador García, Sergio Gil-López, Daniel Molina, Richard Benjamins, et al. Explainable artificial intelligence (xai): Concepts, taxonomies, opportunities and challenges toward responsible ai. *Information fusion*, 58:82–115, 2020. [1](#)
- [3] Sarah Adel Bargal, Andrea Zunino, Vitali Petsiuk, Jianming Zhang, Kate Saenko, Vittorio Murino, and Stan Sclaroff. Guided zoom: Zooming into network evidence to refine fine-grained model decisions. *IEEE Transactions on Pattern Analysis and Machine Intelligence*, 43(11):4196–4202, 2021. [1](#)
- [4] Itay Benou and Tammy Riklin Raviv. Show and tell: Visually explainable deep neural nets via spatially-aware concept bottleneck models. In *Proceedings of the Computer Vision and Pattern Recognition Conference*, pages 30063–30072, 2025. [1](#)
- [5] Chunshui Cao, Xianming Liu, Yi Yang, Yinan Yu, Jiang Wang, Zilei Wang, Yongzhen Huang, Liang Wang, Chang Huang, Wei Xu, et al. Look and think twice: Capturing top-down visual attention with feedback convolutional neural networks. In *Proceedings of the IEEE international conference on computer vision*, pages 2956–2964, 2015. [1](#)
- [6] Aditya Chattopadhyay, Anirban Sarkar, Prantik Howlader, and Vineeth N Balasubramanian. Grad-cam++: Generalized gradient-based visual explanations for deep convolutional networks. In *2018 IEEE winter conference on applications of computer vision (WACV)*, pages 839–847. IEEE, 2018. [2](#) [6](#)
- [7] Hila Chefer, Shir Gur, and Lior Wolf. Generic attention-model explainability for interpreting bi-modal and encoder-decoder transformers. In *Proceedings of the IEEE/CVF international conference on computer vision*, pages 397–406, 2021. [2](#)
- [8] Chaofan Chen, Oscar Li, Daniel Tao, Alina Barnett, Cynthia Rudin, and Jonathan K Su. This looks like that: deep learning for interpretable image recognition. *Advances in neural information processing systems*, 32, 2019. [2](#)
- [9] Julien Colin, Thomas Fel, Rémi Cadène, and Thomas Serre. What i cannot predict, i do not understand: A human-centered evaluation framework for explainability methods. *Advances in neural information processing systems*, 35: 2832–2845, 2022. [2](#)
- [10] Thomas M Cover. *Elements of information theory*. John Wiley & Sons, 1999. [4](#)
- [11] Jia Deng, Wei Dong, Richard Socher, Li-Jia Li, Kai Li, and Li Fei-Fei. Imagenet: A large-scale hierarchical image database. In *2009 IEEE conference on computer vision and pattern recognition*, pages 248–255. Ieee, 2009. [5](#)
- [12] Alexey Dosovitskiy. An image is worth 16x16 words: Transformers for image recognition at scale. *arXiv preprint arXiv:2010.11929*, 2020. [5](#)
- [13] Ian Fischer. The conditional entropy bottleneck. *Entropy*, 22(9):999, 2020. [2](#)
- [14] Arthur Gretton, Olivier Bousquet, Alex Smola, and Bernhard Schölkopf. Measuring statistical dependence with hilbert-schmidt norms. In *International conference on algorithmic learning theory*, pages 63–77. Springer, 2005. [4](#)
- [15] Arthur Gretton, Kenji Fukumizu, Choon Teo, Le Song, Bernhard Schölkopf, and Alex Smola. A kernel statistical test of independence. *Advances in neural information processing systems*, 20, 2007. [4](#)
- [16] Peter Hase, Mohit Bansal, Been Kim, and Asma Ghandeharioun. Does localization inform editing? surprising differences in causality-based localization vs. knowledge editing in language models. *Advances in Neural Information Processing Systems*, 36:17643–17668, 2023. [2](#)
- [17] Kaiming He, Xiangyu Zhang, Shaoqing Ren, and Jian Sun. Deep residual learning for image recognition. In *Proceedings of the IEEE conference on computer vision and pattern recognition*, pages 770–778, 2016. [5](#)
- [18] Gao Huang, Zhuang Liu, Laurens Van Der Maaten, and Kilian Q Weinberger. Densely connected convolutional networks. In *Proceedings of the IEEE conference on computer vision and pattern recognition*, pages 4700–4708, 2017. [5](#)
- [19] Dominik Janzing, Lenon Minorics, and Patrick Blöbaum. Feature relevance quantification in explainable ai: A causal problem. In *International Conference on artificial intelligence and statistics*, pages 2907–2916. PMLR, 2020. [2](#)
- [20] Aditya Khosla, Nityananda Jayadevaprakash, Bangpeng Yao, and Fei-Fei Li. Novel dataset for fine-grained image categorization: Stanford dogs. In *Proc. CVPR workshop on fine-grained visual categorization (FGVC)*, 2011. [5](#)
- [21] Sunnie SY Kim, Nicole Meister, Vikram V Ramaswamy, Ruth Fong, and Olga Russakovsky. Hive: Evaluating the human interpretability of visual explanations. In *European Conference on Computer Vision*, pages 280–298. Springer, 2022. [2](#)
- [22] Polina Kirichenko, Pavel Izmailov, and Andrew Gordon Wilson. Last layer re-training is sufficient for robustness to spurious correlations. *arXiv preprint arXiv:2204.02937*, 2022. [2](#)
- [23] Pang Wei Koh, Thao Nguyen, Yew Siang Tang, Stephen Mussmann, Emma Pierson, Been Kim, and Percy Liang. Concept bottleneck models. In *International conference on machine learning*, pages 5338–5348. PMLR, 2020. [2](#)
- [24] Alex Krizhevsky, Geoffrey Hinton, et al. Learning multiple layers of features from tiny images. 2009. [5](#)
- [25] Evan Z Liu, Behzad Haghgoor, Annie S Chen, Aditi Raghunathan, Pang Wei Koh, Shiori Sagawa, Percy Liang, and Chelsea Finn. Just train twice: Improving group robustness without training group information. In *International Conference on Machine Learning*, pages 6781–6792. PMLR, 2021. [2](#)
- [26] Yiheng Liu, Wengang Zhou, Jianzhuang Liu, Guo-Jun Qi, Qi Tian, and Houqiang Li. An end-to-end foreground-aware network for person re-identification. *IEEE Transactions on Image Processing*, 30:2060–2071, 2021. [2](#)
- [27] Mazda Moayeri, Phillip Pope, Yogesh Balaji, and Soheil Feizi. A comprehensive study of image classification

model sensitivity to foregrounds, backgrounds, and visual attributes. In *Proceedings of the IEEE/CVF Conference on Computer Vision and Pattern Recognition*, pages 19087–19097, 2022. 2

[28] Meike Nauta, Jörg Schlötterer, Maurice Van Keulen, and Christin Seifert. Pip-net: Patch-based intuitive prototypes for interpretable image classification. In *Proceedings of the IEEE/CVF Conference on Computer Vision and Pattern Recognition*, pages 2744–2753, 2023. 2

[29] Tuomas Oikarinen, Subhro Das, Lam M Nguyen, and Tsui-Wei Weng. Label-free concept bottleneck models. *arXiv preprint arXiv:2304.06129*, 2023. 2

[30] Omkar M Parkhi, Andrea Vedaldi, Andrew Zisserman, and CV Jawahar. Cats and dogs. In *2012 IEEE conference on computer vision and pattern recognition*, pages 3498–3505. IEEE, 2012. 5

[31] Andrew Slavin Ross, Michael C Hughes, and Finale Doshi-Velez. Right for the right reasons: Training differentiable models by constraining their explanations. *arXiv preprint arXiv:1703.03717*, 2017. 2

[32] Dawid Rymarczyk, Łukasz Struski, Michał Górszczak, Koryna Lewandowska, Jacek Tabor, and Bartosz Zieliński. Interpretable image classification with differentiable prototypes assignment. In *European Conference on Computer Vision*, pages 351–368. Springer, 2022. 2

[33] Ramprasaath R Selvaraju, Michael Cogswell, Abhishek Das, Ramakrishna Vedantam, Devi Parikh, and Dhruv Batra. Grad-cam: Visual explanations from deep networks via gradient-based localization. In *Proceedings of the IEEE international conference on computer vision*, pages 618–626, 2017. 1, 2, 6

[34] Avanti Shrikumar, Peyton Greenside, and Anshul Kundaje. Learning important features through propagating activation differences. In *International conference on machine learning*, pages 3145–3153. PMLR, 2017.

[35] Karen Simonyan, Andrea Vedaldi, and Andrew Zisserman. Deep inside convolutional networks: Visualising image classification models and saliency maps. *arXiv preprint arXiv:1312.6034*, 2013. 1, 2, 6

[36] Andrew Smart and Atoosa Kasirzadeh. Beyond model interpretability: Socio-structural explanations in machine learning. *AI & SOCIETY*, 40(4):2045–2053, 2025. 1

[37] Daniel Smilkov, Nikhil Thorat, Been Kim, Fernanda Viégas, and Martin Wattenberg. Smoothgrad: removing noise by adding noise. *arXiv preprint arXiv:1706.03825*, 2017. 1, 2

[38] Le Song, Alex Smola, Arthur Gretton, Karsten M Borgwardt, and Justin Bedo. Supervised feature selection via dependence estimation. In *Proceedings of the 24th international conference on Machine learning*, pages 823–830, 2007. 4

[39] Jost Tobias Springenberg, Alexey Dosovitskiy, Thomas Brox, and Martin Riedmiller. Striving for simplicity: The all convolutional net. *arXiv preprint arXiv:1412.6806*, 2014. 5, 6

[40] Mukund Sundararajan, Ankur Taly, and Qiqi Yan. Axiomatic attribution for deep networks. In *International conference on machine learning*, pages 3319–3328. PMLR, 2017. 1, 2, 6

[41] Luming Tang, Menglin Jia, Qianqian Wang, Cheng Perng Phoo, and Bharath Hariharan. Emergent correspondence from image diffusion. *Advances in Neural Information Processing Systems*, 36:1363–1389, 2023. 2

[42] Naftali Tishby, Fernando C Pereira, and William Bialek. The information bottleneck method. *arXiv preprint physics/0004057*, 2000. 2

[43] Catherine Wah, Steve Branson, Peter Welinder, Pietro Perona, and Serge Belongie. The caltech-ucsd birds-200-2011 dataset. 2011. 5

[44] Haofan Wang, Zifan Wang, Mengnan Du, Fan Yang, Zijian Zhang, Sirui Ding, Piotr Mardziel, and Xia Hu. Score-cam: Score-weighted visual explanations for convolutional neural networks. In *Proceedings of the IEEE/CVF conference on computer vision and pattern recognition workshops*, pages 24–25, 2020. 2, 6

[45] Leander Weber, Sebastian Lapuschkin, Alexander Binder, and Wojciech Samek. Beyond explaining: Opportunities and challenges of xai-based model improvement. *Information Fusion*, 92:154–176, 2023. 2

[46] Shirley Wu, Mert Yuksekgonul, Linjun Zhang, and James Zou. Discover and cure: Concept-aware mitigation of spurious correlation. In *International Conference on Machine Learning*, pages 37765–37786. PMLR, 2023. 2

[47] Mert Yuksekgonul, Maggie Wang, and James Zou. Post-hoc concept bottleneck models. *arXiv preprint arXiv:2205.15480*, 2022. 2

[48] Michael Zhang, Nimit S Sohoni, Hongyang R Zhang, Chelsea Finn, and Christopher Ré. Correct-n-contrast: A contrastive approach for improving robustness to spurious correlations. *arXiv preprint arXiv:2203.01517*, 2022. 2

[49] Wenliang Zhao, Yongming Rao, Zuyan Liu, Benlin Liu, Jie Zhou, and Jiwen Lu. Unleashing text-to-image diffusion models for visual perception. In *Proceedings of the IEEE/CVF International Conference on Computer Vision*, pages 5729–5739, 2023. 2

[50] Bolei Zhou, Aditya Khosla, Agata Lapedriza, Aude Oliva, and Antonio Torralba. Learning deep features for discriminative localization. In *Proceedings of the IEEE conference on computer vision and pattern recognition*, pages 2921–2929, 2016. 2